HHS Public Access

Author manuscript

J Neural Eng. Author manuscript; available in PMC 2019 June 01.

Published in final edited form as:

J Neural Eng. 2019 June ; 16(3): 035001. doi:10.1088/1741-2552/ab05b6.

Parallel, minimally-invasive implantation of ultra-flexible neural electrode arrays

Zhengtuo Zhao, **Xue Li**, **Fei He**, **Xiaoling Wei**, **Shengqing Lin**, and **Chong Xie**[*]

Department of Biomedical Engineering, the University of Texas at Austin.

Abstract

Objective.—Implanted microelectrodes provide a unique means to directly interface with the nervous system, but have been limited by the lack of stable functionality. There is growing evidence suggesting that substantially reducing the mechanical rigidity of neural electrodes promotes tissue compatibility and improves their recording stability in both short- and long-terms. However, the miniaturized dimensions and ultraflexibility desired for mitigating tissue responses preclude the probe's self-supported penetration into the brain tissue.

Approach.—Here we demonstrate the high-throughput implantation of multi-shank ultraflexible neural electrode arrays with surgical footprints as small as 200 μm^2 in a mouse model. This is achieved by using arrays of tungsten microwires as shuttle devices, and bio-dissolvable adhesive polyethylene glycol (PEG) to temporarily attach a shank onto each microwire.

Main results.—We show the ability to simultaneously deliver electrode arrays in designed patterns, to adjust the implantation locations of the shanks by need, to target different brain structures, and to control the surgical injury by reducing the microwire diameters to the cellular scale.

Significance.—These results provide a facile implantation method to apply ultraflexible neural probes in scalable neural recording.

1. Introduction

Electrophysiological recording with implanted neural electrodes is of paramount importance in neuroscience [1–3] and holds unique promise for human neuroprosthetics [4–7]. Despite great successes and potential, conventional rigid electrodes such as microwire and microfabricated silicon probes suffer from significant mechanical mismatch with the nervous tissue host and the resulting instability at the interface in both the short and long-terms [8–11].Extensive efforts have been made to reduce the size [12] and mechanical stiffness [8, 13–18] of neural probes for improved biocompatibility and recording reliability. In particular, the recent progress on ultraflexible neural electrodes [19] with drastically reduced probe dimension and mechanical compliance showed seamless tissue integration [20] and great promise of long-term stable recording [20, 21]. However, there is an intrinsic conflict on the requirement of a probe's rigidity between minimal invasiveness and facile insertion into the brain with minimal surgical injury. To eliminate chronic tissue reactions, it is

[*]Correspondence to: chongxie@utexas.edu.

essential to reduce a neural probe's rigidity so that the deformation force of the probe is comparable to the cellular forces in the nervous tissue [20]. However, such ultraflexibility mechanically precludes the probe's self-supported penetration through brain tissue. Implantation techniques that meet the following requirements simultaneously are highly desired: i) to be minimally invasive, having surgical footprint as small as possible to minimize the surgical injury [22–24]; ii) to be scalable and high throughput, so that a large number of electrode contacts at high density can be implanted within a short surgery duration; and iii) to be able to target specific brain regions and depths.

Prior strategies to deliver flexible probes include temporarily altering the probe's rigidity prior to insertion [19, 25, 26], and delivering with a separate rigid shuttle device that is later decoupled from the probe [8, 18, 27–29]. To temporarily alter the probe's rigidity, biodegradable materials, such as polyethylene glycol (PEG) [30] and silk [31], were used to encapsulate and stiffen neural probes to support penetration into the brain tissue, which were then dissolved by the cerebrospinal fluid (CSF) after implantation. Temporarily freezing the probe attached by a small amount of solution was also demonstrated for stereotaxic insertion [19]. Alternatively, novel substrate materials such as mechanically adaptive nanocomposites [14] and shape memory polymer [16] were used to reduce stiffness after implantation. For the shuttle device strategy, a variety of temporary attachment mechanisms such as biodegradable adhesives [8, 27, 28], geometrical anchor [32], and syringe injection [29] have been used. However, most of these implantation methods were designed for sparse implantation of flexible probes that have cross-sectional areas of about 1000 μm^2 or larger, and had limited possibilities to aggressively scale down in dimensions to accommodate increasingly smaller neural probes and denser implantations. Our laboratory has demonstrated ultraflexible nanoelectronic threads (NETs) neural probes with cross-sectional areas ranging from 10 – 100 μm^2 [20, 33]. Therefore, it is critical to develop implantation strategies that offer comparable surgical footprints to the dimension of neural probes. A "needle and thread" mechanism using a microscale shuttle device made of tungsten microwires or carbon fibers successfully delivered NETs at about 200 μm^2 surgical footprint [20], but offered limited throughput and ease of operation, because NET probes were inserted in serial, and each delivery required manual alignment with 1 -μm accuracy.

In this work, we demonstrate a versatile implantation strategy using microwire arrays as the shuttle device, which allows high throughput, parallel insertion of multi-shank NETs with surgical footprints as small as 200 μm^2 per shank (Fig. 1). A typical multi-shank NET probe hosts 32 – 128 contacts on 4 – 8 shanks at the inter-shank spacing of 150 – 400 μ m and an overall thickness of 1 μm [20]. Our implantation scheme aims at delivering all shanks in parallel into the target brain region and depth, while maintaining the mechanical and electrical integrity. To achieve this goal, we design and fabricate a variety of guiding structures such as microtrenches and microconduits to construct tungsten microwire arrays with desired spatial arrangements, and attach the NET probes on the microwire array using a thin layer of PEG. We then stereotaxically insert the assembly into the targeted brain region, and retract the microwire array after the PEG dissolves in the CSF. By using PEG of high molecular weight (35 kDa), we achieve sufficient time duration of attachment that allows for targeting deep brain structures such as hippocampus. Because the PEG adhesion layer used

in the procedure has a sub-micron thickness, the surgical footprint is mostly contributed by the volume of the microwires. We demonstrate successful implantation of multi-shank NETs and reduced tissue damage using tungsten microwires with diameters as small as 12 μm. We present three methods of assembling microwire arrays, using either microfabricated or commercially available guiding structures (Fig. 1). The delivery methods reported in this work use easy-to-access, low-cost supplies and can be readily adapted to the implantation of other ultraflexible neural implants.

2. Methods

2.1 Animal preparation and cranial surgery

Wild-type male mice (C57BJ/6, 8 weeks old, Taconic) were used in the experiments. Mice were housed in the Animal Resources Center at the University of Texas at Austin (UT Austin) at a 12-hour light/dark cycle at 22°C, food and water *ad libitum.* For cranial surgery, the mice were anesthetized with isoflurane (3% for induction, 1–2% for remainder of surgery) in medical-grade oxygen and mounted on a stereotaxic frame (Kent Scientific Inc.). A 3 mm by 3 mm cranial opening was created in the skull using a surgical drill. The dura was carefully removed at the insertion site to facilitate the delivery. After NET probe implantation (described below), the exposed brain and the remaining flexible segment of the NET probe, which connected the bonding pads on the substrate with the electrodes inside the brain, were protected by artificial cerebrospinal fluid (aCSF) and Kwik-Sil adhesive (World Precision Instruments). After the skull was cleaned and dried, a layer of low-viscosity cyanoacrylate was applied over the skull. An initial layer of C&B-Metabond (Parkell Inc.) was applied over the cyanoacrylate and the Kwik-Sil adhesive. A second layer of Metabond was used to cement the coverslip and the carrier chip to the skull (Fig. 1A). All procedures complied with the National Institutes of Health guidelines for the care and use of laboratory animals and were approved by the UT Institutional Animal Care and Use Committee.

2.2 Electrochemical thinning and sharpening of tungsten microwires

Electrochemical etching in 0.8 M KOH solution was used to thin and sharpen tungsten microwires (W5607, Advent Research Materials). Tungsten microwires were cut into appropriate lengths of 4 – 6 mm and mounted on a strip of copper tape with silver epoxy. To thin the wires, a constant voltage of 2.5 V versus a graphite counter electrode (GR001CC, GraphiteStore) was applied to the wires to achieve an appropriate etching speed, while a segment (typically 2 mm long) of the wire was immersed in the etchant. The target diameter was controlled by the etching time. Empirically it takes approximately 1 min to reach the diameter of 25 μm and 2 mins for the diameter of 12 μm. After the wire is thinned to the designated diameter, a sharp tip was formed at the end of the microwire by positioning the tip at the solution-air interface and etching for an extra 3 mins at the same voltage.

2.3 Fabrication and preparation of stand-alone microwire arrays as shuttle devices

Microtrenches of matching spacing as the NET shanks were microfabricated on silicon substrates (4” wafer, 900 nm SiO2, n-type 0.005 V*cm, University Wafer) using standard photolithography. SU-8 photoresist (SU-8 2075, MicroChem Corp.) was spun on the silicon

substrate at 4000 rpm for 45 sec, followed by the standard SU-8 photolithography process which yielded microtrench structures with a depth of 60 μm and width of 50 μm. After hard baking (180 °C, 3h), the 4” wafer was cut into rectangular pieces (3 mm × 4 mm) using dicing saw (7100 Dicing system, ADT), which were used as the carrier chip for shuttle devices. The etched tungsten microwires were placed into the microtrenches manually, resulting in a linear array of microwires at the pitch predefined by the carrier chip. The microwires protruded beyond the edge of the carrier chip by several millimeters depending on the implantation depth. A thin layer of super glue (Loctite) was used to fix microwires in the trenches on the carrier chip without overflowing. Small drops of epoxy (Loctite) were placed on all four corners of the carrier chip to act as spacers between the shuttle device and the NET probe when they were later attached together. The assembled shuttle device was then baked at 180 °C for 30 min for the epoxy to cure.

After the multi-shank NET was fabricated and partially released from the substrate as previously described [20], the shuttle device was aligned with of NET shanks under a stereomicroscope (A60S, Leica Microsystems), with the tip of the microwires protruded the tip of the NET shanks by 10 – 20 μm in length. A flat-end alligator clip was used to hold together the shuttle device and the NET probe, while a small gap was created between them by the epoxy drops at the corners of the shuttle device to prevent damaging the NET probe. The NET substrate was then trimmed to the desired length in deionized water. Subsequently, the NET-shuttle assembly was dipped into the PEG solution (5% w/v, molecular weight of 35 kDa, Alfa Aesar) and slowly pulled out. A 34-gauge syringe needle (O.D. 190 μm) was used to guild NET shanks to attach onto each microwire with the assistance of surface tension [34]. After the attachment, additional PEG was applied between the shuttle device carrier chip and the NET substrate to attach them together. The clip was then removed, and the assembled device was allowed to dry in air. The design and implementation of this procedure are shown in Fig. 2.

2.4 Stereotaxic implantation of NET probes with stand-alone microwire arrays as shuttle devices

The assembled NET-shuttle device pair was attached to a micromanipulator on the stereotaxic frame with the back of the NET substrate contacting the tape. The micromanipulator was manually controlled to insert the NET-microwire array into the designated region of the mouse brain. The three-dimensional (3D) coordinates of the arrays were measured (Digital lab standard, Stoelting Co.) during insertion for the control of depth and speed.

After the NET-microwire array reached the target position, a small drop of glue was gently placed on the shuttle device carrier chip. A customized stainless steel pole (1 mm in diameter) mounted on the second micromanipulator on the stereotaxic frame was manually controlled to approach the glue on the shuttle device carrier chip and stayed in contact as the glue cured. After the glue completely cured and the PEG between NET shanks and microwires was dissolved by the tissue fluid, sterile phosphate buffered saline (PBS) was applied to dissolve the PEG that attached the shuttle carrier chip with the NET substrate. The shuttle device was then carefully retracted from the tissue using the second

micromanipulator, leaving the detached NETs in the implantation sites. The typical extraction speed was about 1 mm/s. In this study, NET probes were implanted in 3 mice with the stand-alone microwire array.

2.5 Microwire assembly using integrated microtrench arrays on the NET substrate

At the end of the NET fabrication, an extra photolithography process was used to define microtrench arrays using SU-8 photoresist (SU-8 2075, MicroChem Corp.) similarly as described in the precious sections. After connectors were soldered on the contact pads, etched tungsten microwires in diameters of 12, 25 or 50 μm and length of 4 – 6 mm were manually placed into the microtrenches. The front end of the microwires were aligned to the end of the NET shanks, while the rear end of the microwires were at least 2 mm exceeding the connector. The microtrenches were then partially filled with PEG solution to fix the microwires in place. PEG is used in this step to allow the microwires to be released and retracted after surgical insertion. A flat silicon chip was placed on top of the microtrenches and fixed on the NET substrate by epoxy, which acted as a cap to restrain the out-of-plane motions of the microwires during retraction. The NETs were then released and attached onto the microwires in the PEG solution using the same procedure as described in 2.3. The assembled device was ready for implantation after dried in air. The design and implementation of this procedure are shown in Fig. 3.

2.6 Assembling microwire arrays guided by microconduit arrays

Polytetrafluoroethylene tubes (Sub-lite-wall tubing, O.D. 200 μm, I. D. 100 μm, Zeus) of a length of 6 mm were manually stacked to form a variety of structures, including linear, rectangular and triangular arrays. Epoxy (Loctite) was applied to permanently fix the structures. Pre-cut straight tungsten microwires the same as used in the previous method were inserted into all or a selection of the conduits. The microwires protruded the tube edge by 3–5 mm on both ends while PEG solution was applied at the rear end of the conduits to temporarily fix the microwires. The microconduit array was then mounted on the NET substrate using Epoxy (Loctite), and aligned under stereomicroscope so that the lateral position of individual microwires best matched the positions of NET shanks and the microwires protruded the end of the NET shanks by 50 – 100 μm. The flexible segment of NETs was then released and attached onto the microwires using PEG solution as described in 2.3. The assembled device was ready for implantation after dried in air. The design and implementation of this procedure are shown in Fig. 4.

2.7 Stereotaxic implantation of NET arrays with integrated microwire arrays

The assembled NET device in 2.5 and 2.6 was attached onto a micromanipulator on the stereotaxic frame, with the back of the NET substrate facing the micromanipulator. The micromanipulator was manually controlled to insert the NET-microwire array into the designated region of the mouse brain similarly as described above. After the NET probe reached the target position and depth, sterile PBS was applied on the rear end of the assembly to dissolve the PEG and release the microwires from the microconduit or microtrenches, while the tissue fluid in brain dissolved the PEG and released NET shanks from the microwires. After PEG was fully dissolved on both ends, which typically took less than 2 minutes, individual microwires were picked up from the rear end by tweezers and

manually retracted one at a time, leaving NETs implanted at the target positions. In this study, NET probes were implanted in 5 mice with the integrated microtrench array and 3 mice with the microconduit array.

2.8 Insertion injury test

The test of insertion tissue damage was performed at primary visual cortex with tungsten microwires' diameters of 12 μm, 25 μm, and 50 μm etched and sharpened as described in 2.2. The insertion speed was approximately 1 mm/s, and the insertion depth was 1 mm. For quantitative comparison, the surface area of the central bleeding spot was measured for each insertion site using ImageJ. NET probes were retracted with the microwires for the ease of the measurement. The insertions were repeated and the bleeding areas were averaged at 12 separate locations in two mice for microwires at diameters of 12 and 25 μm, and at 20 locations in two mice for microwires at the diameter of 50 μm.

2.9 Electrophysiological recording and impedance measurement

Multi-shank NET probes were implanted into the primary somatosensory cortex and primary motor cortex in the mouse brain at depths ranging from 700 μm to 1 mm at the tip. Intan 64-channel RHD2164 evaluation system (Intan Technologies) was used for neural signal acquisition using sampling rate of 20 kHz. The recording was performed from awake mice head fixed on a custom-made treadmill ten days post implantation. Common median referencing [35] was applied to the raw data to reduce the common mode noise such as motion artifacts, etc. Spike sorting was performed with Offline Sorter (Plexon). In vivo impedance was measured with the same system at 1 kHz prior to each recording session. The impedance was also measured with the same system in PBS solution prior to implantation. Single unit was identified based on the criteria that the fraction of spikes with inter-spike intervals under 2 ms were less than 1% of the total firing. [36]

2.10 Histology

The mice were perfused intracardially using oxygenated aCSF at 4°C, then with a 4% paraformaldehyde solution in 0.02 M PBS. 30% sucrose/4% paraformaldehyde solution was used to soak the brains overnight. Brain tissue was sliced using a Leica CM1950 cryostat (Leica Microsystems) into 20 μm slices, which were then washed for three 5-minute sessions before incubated for 30 minutes in a sodium citrate solution (85°C to 95°C, 0.01 M in H2O) for antigen retrieval. The slices were washed again for three 5-minute sessions, incubated in a blocking solution, permeabilized [0.5% Triton X-100 and 10% normal goat serum (Sigma-Aldrich) in PBS] for 3 hours at 25°C, washed again for four 5-minute sessions, then incubated with the one-step fluorophore-conjugated antibodies at 4°C for 24 hours. To immunochemically stain neurons, Alexa Fluor 568–conjugated anti-NeuN antibody (ab207282, abcam) was used. In this study, the evaluation of the insertion depth in cortex, in the subcortical region (hippocampus), and the examination of tissue-probe interface were performed in two, one, and one mouse brains,respectively.

3. Results

3.1 Implantation of NET arrays

To accurately implant multi-shank NETs with minimal surgical injury, the microwires must be highly straight, parallelly aligned, and as thin as possible. Using the methods described above, we constructed linear microwire arrays as shuttle devices for parallel implantation of NET probes, shown in Fig. 2 and 3. We fabricated microtrenches on a stand-alone silicon chip (Fig. 2A) as aligning structures for the microwires. The pitch of the microtrenches matched the intershank spacings of NET probes at 400 μm, 250 μm or 150 μm. We found that tungsten microwires at the diameter of 50 μm, among all commercially available microwires we have tested, had the best straightness and yielded the most predictable etching results, from which we generated straight microwires with thinned segments at the diameters of 25 μm and sharpened tips (Fig. 2B). We used a surface-tension assisted manual process (see methods) to achieve nearly conformal attachment of NET shanks on the microwires with PEG working as a water-soluble adhesive (Fig. 2C-E). Fig. 2F-G illustrate typical implantation of NETs in mouse brains with the microwire-shuttle device.

As an alternative solution, we fabricated microtrenches directly on the NET substrate (Fig. 3A) and used them to guide the microwire alignment. We show aligning (Fig. 3B) and attaching (Fig. 3C) of eight-shank NETs onto microwire linear arrays with matching pitches. Using simplified stereotaxic insertion and retraction procedures (see methods), we demonstrated the implantation of 8-shank NETs in the mouse cortex at 150 μm spacing (Fig. 3D, E).

These procedures yielded repeatable assembly of NET-shuttle device with predictable arrangement. We used the NET probe with 150 μm shank pitch to quantify the spatial regularity, which has the smallest shank spacing among all our designs and is the most susceptible to wire deformation. We assembled 24 NET shanks with shuttle devices, from which we determined the discrepancy from expected outcome. The angle deviation of the shanks from the guiding structures measured 0.15±0.11 °, and the averaged center-to-center distance measured 147 ±13 μm. (Mean and standard deviation were used for all statistical analysis in this work.) The spatial arrangement of the shanks in the microwire-NET assembly was mostly preserved after the implantation. For two groups of 24 shanks per group at the shank spacing of 400 μm and 150 μm, the average values of the shank spacing after implantation were 400 ± 22 μm and 156 ±18 μm, respectively.

Besides in-line implantation of multi-shank NETs, we further demonstrated that a microconduit shuttle device made from off-the-shelf components can facilitate the implantation of NETs in various arrangements (Fig. 4). To construct the shuttle device, we stacked microtubes in a variety of patterns, such as linear, triangular or rectangular arrays, and inserted microwires in all or a selection of them (Fig. 4A-C). We then attached NETs onto the microwires (see methods). These versatile arrangements allowed NETs to be implanted in parallel with customized site and depth arrangement, which help optimize the recording coverage and/or avoid major surface blood vessel (Fig. 4D).

3.2 Minimized surgical injury

To reduce the surgical injury during implantation, we minimized the overall cross-sectional footprint of the NET-shuttle assembly, which is determined by the diameter of the microwire and the thickness of the PEG adhesive in addition to the size of NETs. We chose to use PEG solution at 5% w/v and the molecular weight of 35 kDa for its desired balance of sufficiently long dissolving time in tissue (discussed later), relatively low viscosity for the ease of handling, and sub-micron coating thickness. Scanning electron microscopy (SEM) images (Fig. 5A-C) confirmed that the PEG coating added negligible volume to the NET-shuttle assemblies. To further reduce the tissue displacement during implantation, we used microwires with reduced diameters of 12 and 25 μm that were electrochemically etched and sharpened from microwires 50 μm in diameter (Fig. 5D-F, see methods). The angle of the tips varies with the diameter of the shuttle wires, measured 8.5 ± 1.5°, 11.3 ± 2.1°, and 15.2 ± 1.9° for 12 μm, 25 μm, and 50 μm microwires respectively. Microwires of all dimensions supported parallel implantation of NET arrays in the mouse cortex. The surface bleeding induced by the implantation, which was measured by the area covered by blood after retraction of microwires, significantly decreased with the diameter of the microwires (Fig. 5G-J).

3.3 Impedance and unit recording of implanted NET electrodes

Ultraflexible NETs are vulnerable to forceful manipulations. Our methods kept their structural and functional integrity during assembly and implantation. In a group 6 multi-shank NET probes with 140 contacts in total, we characterized the electrodes by measuring the impedance at 1 kHz before and after implantation (Fig. 6A). All contacts remained connected and the average impedance had a minor increase of 50 – 300 kΩ from the *in vitro* measurements before implantation. We attribute this increase to the tissue-electrode interface impedance [37]. In Figure 6B-D, we showcase the typical recording performance of a 32-ch NET probe implanted in mouse motor cortex using this method. All 32 channels were confirmed to be connected by impedance check. We yielded 33 single units from the recording with an average amplitude 107.15 ± 44.68 μV and noise level 21.12 ± 1.67 μV ten days post implantation.

3.4 Control on the insertion depth

Precisely controlling the insertion depth of NETs is critical to reach the designated implantation target. We found that precise insertion depth could be achieved as long as the NET-shuttle assembly reached the targeted stereotaxic coordinates before the PEG was fully dissolved. Because we cannot directly observe the dissolution of PEG, we typically waited for a sufficiently long time (2 mins) before we proceeded. We performed *in vitro* and *in vivo* tests to determine the precision of targeting specific implantation depths. In 0.5% agarose gel, which had similar mechanic properties as mouse brain [39], we targeted the insertion depth of 2 mm at an insertion speed of 100 μm/s, and achieved 2.017 mm ± 34 μm (n=10) (Fig. 7A-C). In the *in vivo* tests, we targeted the depth of 1 mm in the mouse primary somatosensory cortex (S1) at the speed of 300 μm/s. The experiment was conducted in two mice, with 3 and 4 shanks inserted in each animal respectively. We determined the implantation depth by postmortem histological tissue examination (Fig. 7D) and achieved

1.029 mm ± 55 μm (n=7). We also targeted the mouse hippocampus at depth of 2 mm and at the speed of 1 mm/s. We attempted to insert 20 shanks in total, and successfully implanted all with an average tip depth of 2.062 mm ± 108 μm (N=20). Figure 7E shows a slice highlighting 5 shanks implanted in hippocampus.

3.5 Post-Mortem tissue-probe interface

To further evaluate the implantation outcome, we examined the tissue-probe interface using postmortem histology two months after implantation (see Methods). Fig. 8 shows representative images of a tissue slice from the mouse primary somatosensory cortex (S1) at depth about 400 μm where an 8-shank NET probe was implanted at the inter-shank spacing of 250 μm. Normal neuronal density and morphology were observed in the close vicinity of the NETs, including regions between nearby NET shanks. These observations are qualitatively consistent with our previous studies on chronically implanted individual NET shanks [20] and NET linear arrays [33]. The long-term outcome of this implantation method will be further investigated in our future studies.

Discussion

We chose to use tungsten microwires to construct the shuttle devices in this work. First, they have sufficiently high Young's modulus (411 GPa), so that microwires with cross-sectional area as small as 110 μm^2 (12 μm in diameter) have adequate mechanical strength to penetrate brain tissues, which allows for reduced surgical footprints (less than 200 μm^2, shuttle-NET combined) comparing with other commonly used materials such as silicon [28]. Secondly, they have high tensile strength (1.5 GPa) and are robust during handling. Thirdly, they are commercially available at a variety of diameters and at low cost. The implantation techniques can be readily adapted using other high Young's modulus materials such as carbon fibers, SiC fibers, and diamond microbeams.

The smallest inter-shank spacing we demonstrated using the microtrenches guided microwire arrays was 150 μm, which is comparable to the closest spaced silicon neural probes [38, 40] and Utah arrays [38]. When using microconduit arrays to guide microwire alignment, the spacing is determined by the outer diameters of the tubes, which ranges from 150 μm to millimeters for off-the-shelf tubes.

The presented method involves considerable manual manipulations. On average, it took 20–30 min to assemble one device including microwire placement, NET attachment and additional packaging. The overall success rate was about 90%, and most of the failure came from mechanically tearing off the shanks when trimming the NET substrate and attaching NETs on the microwires. Once NETs are successfully assembled with shuttle devices, their implantation yield can reach nearly 100% by trained operators.

There are a few limitations in the current technique that can be improved in the future development. First, the PEG used in this method has relatively short dissolution time in tissues, which excludes extremely slow insertion speeds (<5 μm/s). Further, because the PEG coating encapsulated recording sites during insertion, it was difficult to record the neural activity during insertion, which was often used to target and verify the implantation

depth. This limitation can be potentially improved by choosing adhesives with longer dissolution time such as silk, and applying it only at the tip of the probe instead of coating the entire shank. Second, the throughput, yield, and consistency of the assembly process can be improved by replacing some or all of the manual manipulation with automatic procedures.

Acknowledgments

We thank the Microelectronics Research Center at UT Austin for the microfabrication facility and support, and the Animal Resources Center at UT Austin for animal housing and care. This work was supported by National Institute of Neurological Disorders and Stroke through R01NS102917, by the UT BRAIN Seed grant award #365459, by the Welch Foundation Research grant #F-1941–20170325, and by DOD CDMRP under award no. W81XWH-16–1-0580.

References

[1]. Alivisatos AP, Chun M, Church GM, Greenspan RJ, Roukes ML and Yuste R 2012 The brain activity map project and the challenge of functional connectomics Neuron 74 970–4 [PubMed: 22726828]

[2]. Shen H 2013 Neurotechnology: BRAIN storm Nature 503 26–8 [PubMed: 24201265]

[3]. Spira ME and Hai A 2013 Multi-electrode array technologies for neuroscience and cardiology Nat. Nanotechnol. 8 83–94 [PubMed: 23380931]

[4]. Birmingham K, Gradinaru V, Anikeeva P, Grill WM, Pikov V, McLaughlin B, Pasricha P, Weber D, Ludwig K and Famm K 2014 Bioelectronic medicines: a research roadmap Nat. Rev. Drug. Discov. 13 399–400 [PubMed: 24875080]

[5]. Collinger JL, Foldes S, Bruns TM, Wodlinger B, Gaunt R and Weber DJ 2013 Neuroprosthetic technology for individuals with spinal cord injury J. Spinal. Cord. Med. 36 258–72 [PubMed: 23820142]

[6]. Nicolelis MAL 2001 Actions from thoughts Nature 409 403–7 [PubMed: 11201755]

[7]. Perlmutter JS and Mink JW 2006 Deep brain stimulation Annu. Rev. Neurosci. 29 229–57 [PubMed: 16776585]

[8]. Kim TI, McCall JG, Jung YH, Huang X, Siuda ER, Li YH, Song JZ, Song YM, Pao HA, Kim RH, Lu CF, Lee SD, Song IS, Shin G, Al-Hasani R, Kim S, Tan MP, Huang YG, Omenetto FG, Rogers JA and Bruchas MR 2013 Injectable, Cellular-Scale Optoelectronics with Applications for Wireless Optogenetics Science 340 211–6 [PubMed: 23580530]

[9]. Kozai TDY, Du ZH, Gugel ZV, Smith MA, Chase SM, Bodily LM, Caparosa EM, Friedlander RM and Cui XT 2015 Comprehensive chronic laminar single-unit, multi-unit, and local field potential recording performance with planar single shank electrode arrays J. Neurosci. Meth. 242 15–40

[10]. Polikov VS, Tresco PA and Reichert WM 2005 Response of brain tissue to chronically implanted neural electrodes J. Neurosci. Meth. 148 1–18

[11]. Rousche PJ, Normann RA 1998 Chronic recording capability of the Utah Intracortical Electrode Array in cat sensory cortex J. Neurosci. Meth. 82 1–15

[12]. Kozai TDY, Langhals NB, Patel PR, Deng XP, Zhang HN, Smith KL, Lahann J, Kotov NA and Kipke DR 2012 Ultrasmall implantable composite microelectrodes with bioactive surfaces for chronic neural interfaces Nat. Mater. 11 1065–73 [PubMed: 23142839]

[13]. Delivopoulos E, Chew DJ, Minev IR, Fawcett JW and Lacour SP 2012 Concurrent recordings of bladder afferents from multiple nerves using a microfabricated PDMS microchannel electrode array Lab Chip 12 2540–51 [PubMed: 22569953]

[14]. Harris JP, Capadona JR, Miller RH, Healy BC, Shanmuganathan K, Rowan SJ, Weder C and Tyler DJ 2011 Mechanically adaptive intracortical implants improve the proximity of neuronal cell bodies J. Neural. Eng. 8

[15]. Jeong JW, Shin G, Park S II, Yu KJ, Xu LZ and Rogers JA 2015 Soft Materials in Neuroengineering for Hard Problems in Neuroscience Neuron 86 175–86 [PubMed: 25856493]

[16]. Simon DM, Charkhkar H, St John C, Rajendran S, Kang T, Reit R, Arreaga-Salas D, McHail DG, Knaack GL, Sloan A, Grasse D, Dumas TC, Rennaker RL, Pancrazio JJ and Voit WE 2017 Design and demonstration of an intracortical probe technology with tunable modulus J. Biomed. Mater. Res. A 105 159–68 [PubMed: 27615364]

[17]. Rousche PJ, Pellinen DS, Pivin DP, Williams JC, Vetter RJ and Kipke DR 2001 Flexible polyimide-based intracortical electrode arrays with bioactive capability IEEE T. Bio-Med. Eng. 48 361–71

[18]. Sohal HS, Jackson A, Jackson R, Clowry GJ, Vassilevski K, O'Neill A and Baker SN 2014 The sinusoidal probe: a new approach to improve electrode longevity Front. Neuroeng. 7 10 [PubMed: 24808859]

[19]. Xie C, Liu J, Fu TM, Dai XC, Zhou W and Lieber CM 2015 Three-dimensional macroporous nanoelectronic networks as minimally invasive brain probes Nat. Mater. 14 1286–92 [PubMed: 26436341]

[20]. Luan L, Wei XL, Zhao ZT, Siegel JJ, Potnis O, Tuppen CA, Lin SQ, Kazmi S, Fowler RA, Holloway S, Dunn AK, Chitwood RA and Xie C 2017 Ultraflexible nanoelectronic probes form reliable, glial scar-free neural integration Sci. Adv. 3

[21]. Fu TM, Hong GS, Zhou T, Schuhmann TG, Viveros RD and Lieber CM 2016 Stable long-term chronic brain mapping at the single-neuron level Nat. Methods 13 875 [PubMed: 27571550]

[22]. Bjornsson CS, Oh SJ, Al-Kofahi YA, Lim YJ, Smith KL, Turner JN, De S, Roysam B, Shain W and Kim SJ 2006 Effects of insertion conditions on tissue strain and vascular damage during neuroprosthetic device insertion J. Neural. Eng. 3 196–207 [PubMed: 16921203]

[23]. Kozai TDY, Gugel Z, Li X, Gilgunn P J, Khilwani R, Ozdoganlar OB, Fedder GK, Weber DJ and Cui XT 2014 Chronic tissue response to carboxymethyl cellulose based dissolvable insertion needle for ultra-small neural probes Biomaterials 35 9255–68 [PubMed: 25128375]

[24]. Potter KA, Buck AC, Self WK and Capadona JR 2012 Stab injury and device implantation within the brain results in inversely multiphasic neuroinflammatory and neurodegenerative responses J. Neural. Eng. 9

[25]. Hassler C, Boretius T and Stieglitz T 2011 Polymers for Neural Implants (vol 49, pg 18, 2011) J. Polym. Sci. Pol. Phys. 49 255–

[26]. Khaled I, Elmallah S, Cheng C, Moussa WA, Mushahwar VK and Elias AL 2013 A Flexible Base Electrode Array for Intraspinal Microstimulation IEEE T. Bio-Med. Eng. 60 2904–13

[27]. Felix SH, Shah KG, Tolosa VM, Sheth HJ, Tooker AC, Delima TL, Jadhav SP, Frank LM and Pannu SS 2013 Insertion of Flexible Neural Probes Using Rigid Stiffeners Attached with Biodissolvable Adhesive J. Vis. Exp.

[28]. Kozai TDY and Kipke DR 2009 Insertion shuttle with carboxyl terminated self-assembled monolayer coatings for implanting flexible polymer neural probes in the brain J. Neurosci. Meth. 184 199–205

[29]. Liu J, Fu TM, Cheng ZG, Hong GS, Zhou T, Jin LH, Duvvuri M, Jiang Z, Kruskal P, Xie C, Suo ZG, Fang Y and Lieber CM 2015 Syringe-injectable electronics Nat. Nanotechnol. 10 629 [PubMed: 26053995]

[30]. Takeuchi S, Yoshida Y, Ziegler D, Mabuchi K and Suzuki T 2004 Parylene flexible neural probe with micro fluidic channel Proc. IEEE Micr. Elect. 208–11

[31]. Wu F, Tien LW, Chen FJ, Berke JD, Kaplan DL and Yoon E 2015 Silk-Backed Structural Optimization of High-Density Flexible Intracortical Neural Probes J. Microelectromech. S. 24 62–9

[32]. Kim BJ, Kuo JTW, Hara SA, Lee CD, Yu L, Gutierrez CA, Hoang TQ, Pikov V and Meng E 2013 3D Parylene sheath neural probe for chronic recordings J. Neural. Eng. 10

[33]. Wei XL, Luan L, Zhao ZT, Li X, Zhu HL, Potnis O and Xie C 2018 Nanofabricated Ultraflexible Electrode Arrays for High-Density Intracortical Recording Adv. Sci. 5

[34]. Zhao ZT, Luan L, Wei XL, Zhu HL, Li X, Lin SQ, Siegel JJ, Chitwood RA and Xie C 2017 Nanoelectronic Coating Enabled Versatile Multifunctional Neural Probes Nano Lett. 17 4588–95 [PubMed: 28682082]

[35]. Rolston JD, Gross RE, Potter SM 2009 Common median referencing for improved action potential detection with multielectrode arrays. In Proceedings of the 2009 Annual International

Conference of the IEEE Engineering in Medicine and Biology Society, Minneapolis, MN, USA 3–6 1604–1607

[36]. Dhawale AK, Poddar R, Wolff SB, Normand VA, Kopelowitz E, Olveczky BP 2017 Automated long-term recording and analysis of neural activity in behaving animals Elife 6

[37]. Wei XF and Grill WM 2009 Impedance characteristics of deep brain stimulation electrodes in vitro and in vivo J. Neural. Eng. 6

[38]. Maynard EM, Nordhausen CT and Normann RA 1997 The Utah Intracortical Electrode Array: A recording structure for potential brain-computer interfaces Electroen. Clin. Neuro. 102 228–39

[39]. Pervin F. C W W. Dynamic Behavior of Materials; Conference Proceedings of the Society for Experimental Mechanics Series; Springer; 2011.

[40]. Rios G, Lubenov EV, Chi D, Roukes ML and Siapas AG 2016 Nanofabricated Neural Probes for Dense 3-D Recordings of Brain Activity Nano Lett. 16 6857–62 [PubMed: 27766885]

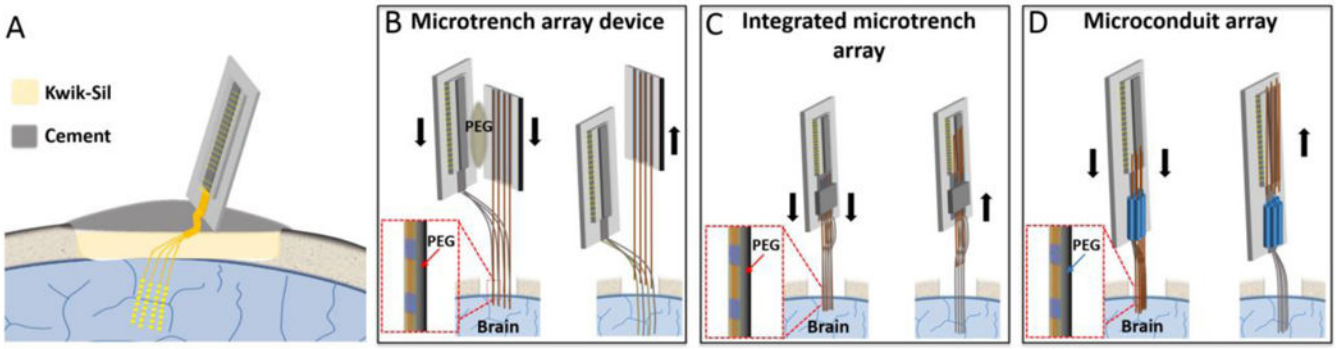

Figure 1:

Schematics of the implantation methods for NET probes. (A) Sketch showing an implanted multi-shank NET and the skull fixation of the back-end carrier chip. (B – D) Sketches showing the implantation procedures for three methods described in the paper, all using pre-aligned microwires as the shuttle devices and a temporary attachment mechanism by dissolvable adhesive.

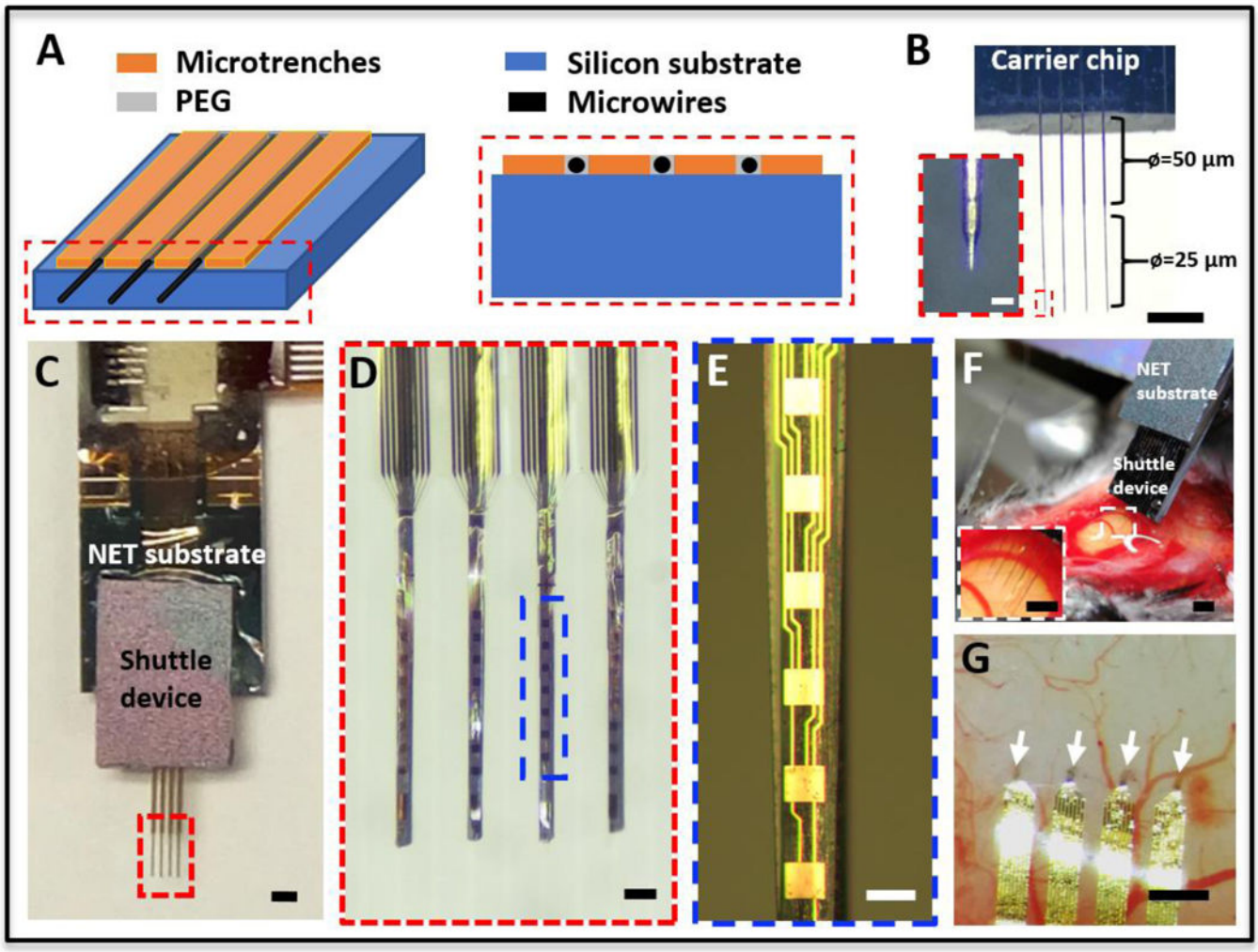

Figure 2:

Stand-alone microwire arrays and NET implantation. (A) Sketches of the shuttle device showing the microfabricated trenches and the aligned microwires placed in between. (B) Photograph of a shuttle device composed of a linear array of microwires aligned to the microtrenches. The last segment of the microwire was etched from a diameter of 50 µm to 25µm. Inset shows the zoom-in view of the dashed box. (C) Photograph of assembled NET-shuttle device. (D) Zoom-in view of the dashed box in C, showing the alignment of NETs on the microwire array. (E) Zoom-in view of the dashed box in D. (F) Photograph showing the stereotaxic insertion of the NET-shuttle device pair. (G) Photograph of the implanted multishank NETs at inter-shank spacing of 400 µm. The arrows point to the four implantation locations. Scale bars: 500 µm (B, C, F, F inset and G); 100 µm (D); 50 µ m (E), 25 µm (B inset).

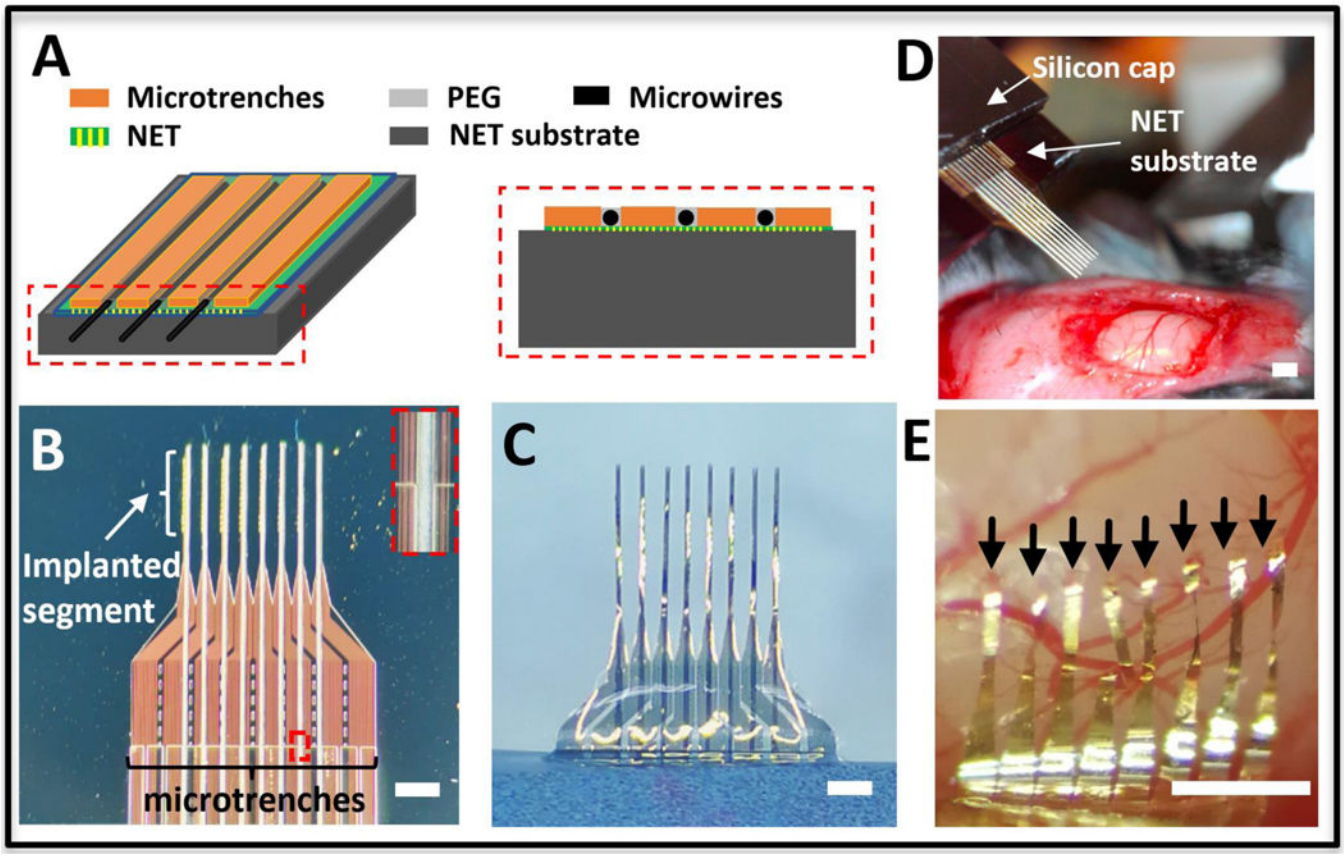

Figure 3:

Integrated microwire array and NET implantation. (A) Sketches showing the microfabricated trenches on top of the NET substrate (left) and the cross-sectional view (right). (B) Photograph of integrated microtrenches and microwires aligned on top of 8-shank NET probe on the substrate at the inter-shank spacing of 250 μm. Inset shows the zoom-in view of the dashed box. (C) Photographs showing the back side of assembled NET-microwire arrays after NETs were released from the substrate. (D) Photograph showing the stereotaxic insertion of the NET-microwire array. (E) Photograph of the implanted NET probe after microwires were retracted. The arrows point to the implantation sites of eight NETs at pitch of 150 μm. Scale bars: 500 μm.

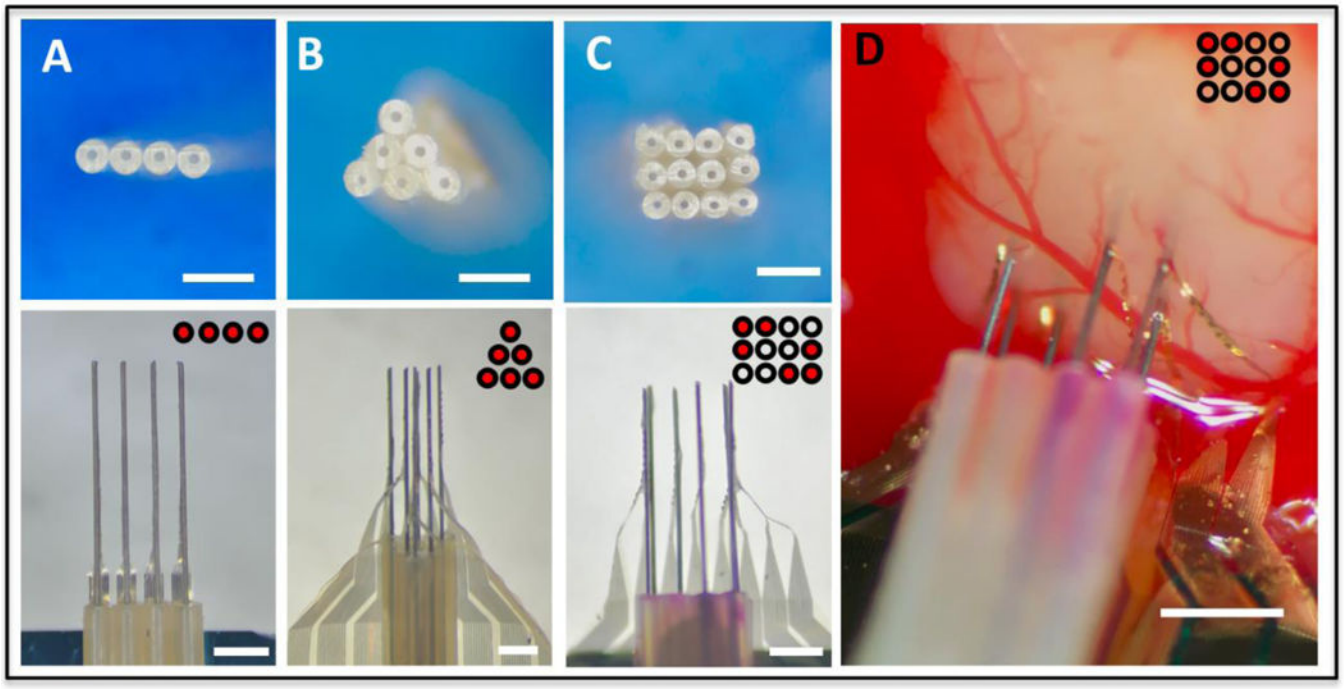

Figure 4:

Versatile implantation using shuttle devices made by microtubes. (A-C) Photographs showing various arrangements of microwires aligned by microtube stacks. Examples of linear (A), triangular (B) arrays, and a customized selection in a rectangular structure (C) were shown. Top: microtubes stacked in desired patterns. Bottom: NETs attached to the shuttle device and ready for implantation. (D) Photograph of a representative implantation using tube guided microwire array, for which the arrangement of microwires was customized to avoid a major blood vessel in the primary visual cortex (V1) of mouse brain. Insets for all panels illustrate the patterns of the microtubes (black circles) and the ones with inserted microwires (red dots). Scale bars: 500 μm.

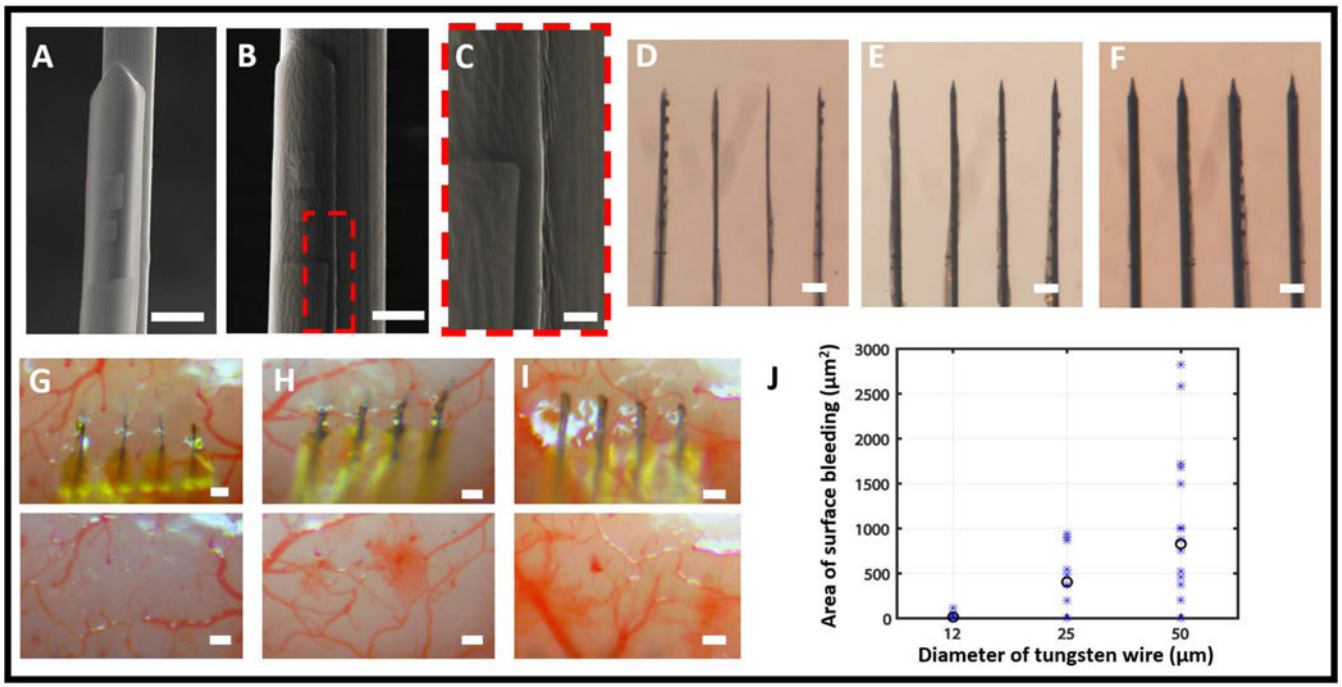

Figure. 5:

Shuttle microwires of different diameters and their insertion damage. (A – C) SEM images showing NETs attached to microwires with diameters of 25 μm (A) and 50 μm (B, C) using PEG. (C) is the zoomed-in view of the dashed box in B. The PEG layers, in all images, added negligible volume to the assembly. (D – F) Photographs showing NET arrays attached on microwires with diameters of 12 μm (D), 25 μm (E), and 50 μm (F). (G – I) Representative photographs showing *in vivo* insertion of NETs using microwires with diameters of 12 μm (G), 25 μm (H) and 50 μm (I), and the corresponding brain surface after the retraction of the wire. (J) The area of bleeding observed from brain surface for the three diameters of microwires. All trials (asteroid) and their averaged value (circle) are plotted. Scale bars: 25 μm (A and B); 5 μm (C), 100 μm (D-F and G-I).

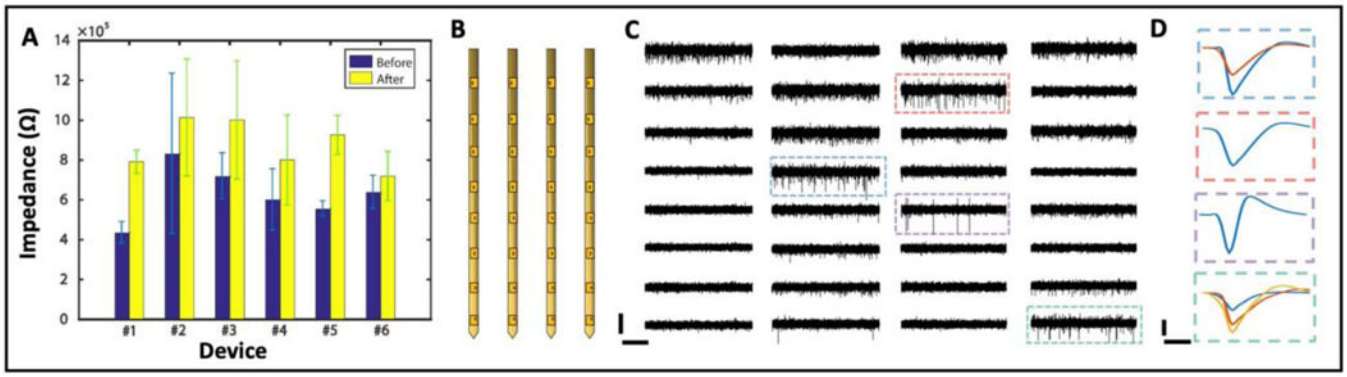

Figure 6:

Electrical characterization of implanted NETs. (A) Impedance before and after implantation for 6 32-channel NETs. (B) Sketch of the 32-channel NET array hosting 4 shanks with 8 recording sites on each shank. (C) 2-s recording traces from a NET array as sketched in B. Scale bar: 100 μV (vertical) and 0.5 s (horizontal). (D) Representative averaged waveforms from 4 electrodes indicated by dashed boxes in C. Scale bar: 50 μV (vertical) and 0.5 ms (horizontal).

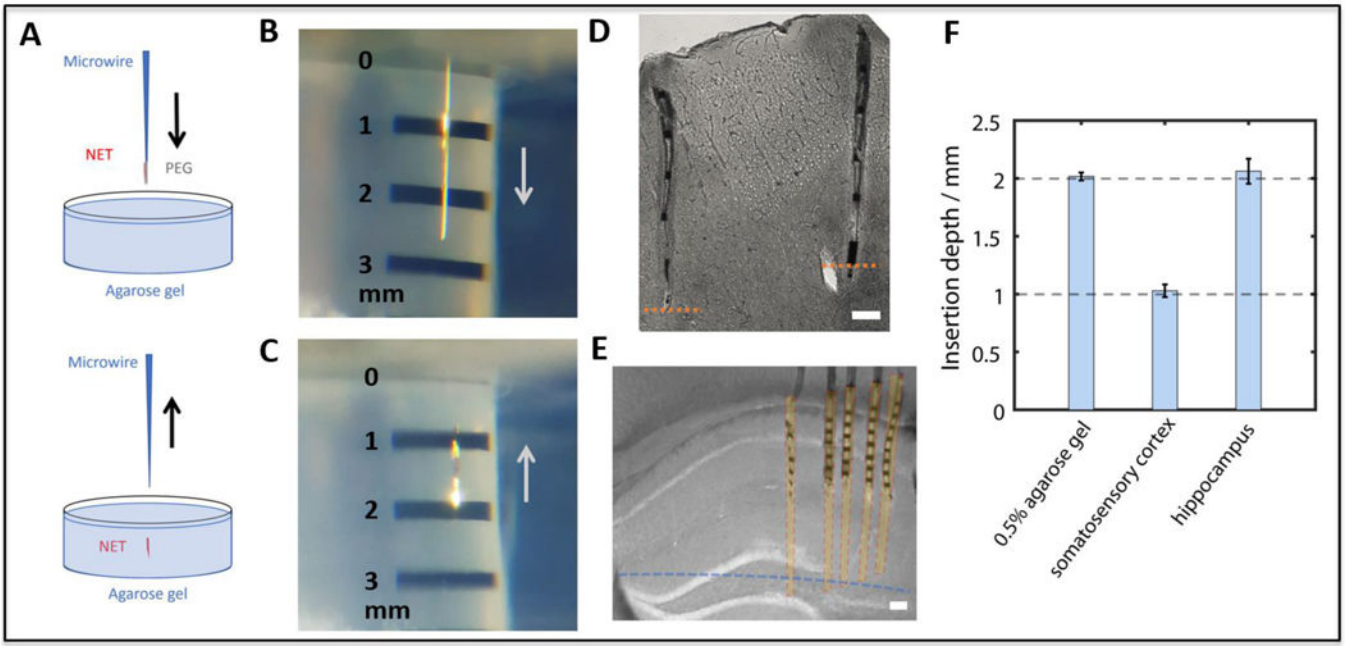

Figure 7:

In vitro and *in vivo* tests of insertion depth accuracy. (A) Sketch illustrating the *in vitro* test setup in the agarose gel. (B, C) Insertion of NETs in the agarose gel targeting the depth of 2 mm. (D) Stitched image of a brain slice showing two representative implanted NETs in the mouse somatosensory cortex (S1) at the designated depth of 1 mm. Orange dash lines mark the measured depth of 1mm from the brain surface. (E) Bright-field image of a brain slice with implanted NETs in mouse hippocampus. The blue dash line marks the measured depth of 2mm from the brain surface. Part of the shanks were sliced off during sample preparation. Yellow shaded areas mark the estimated coverage of the recording regions. (F) Measured insertion depths and standard deviation in gel, cortex and hippocampus. Insertions targeted depths at 2 mm in gel and hippocampus, and at 1 mm in somatosensory cortex. Scale bars: 100 μm.

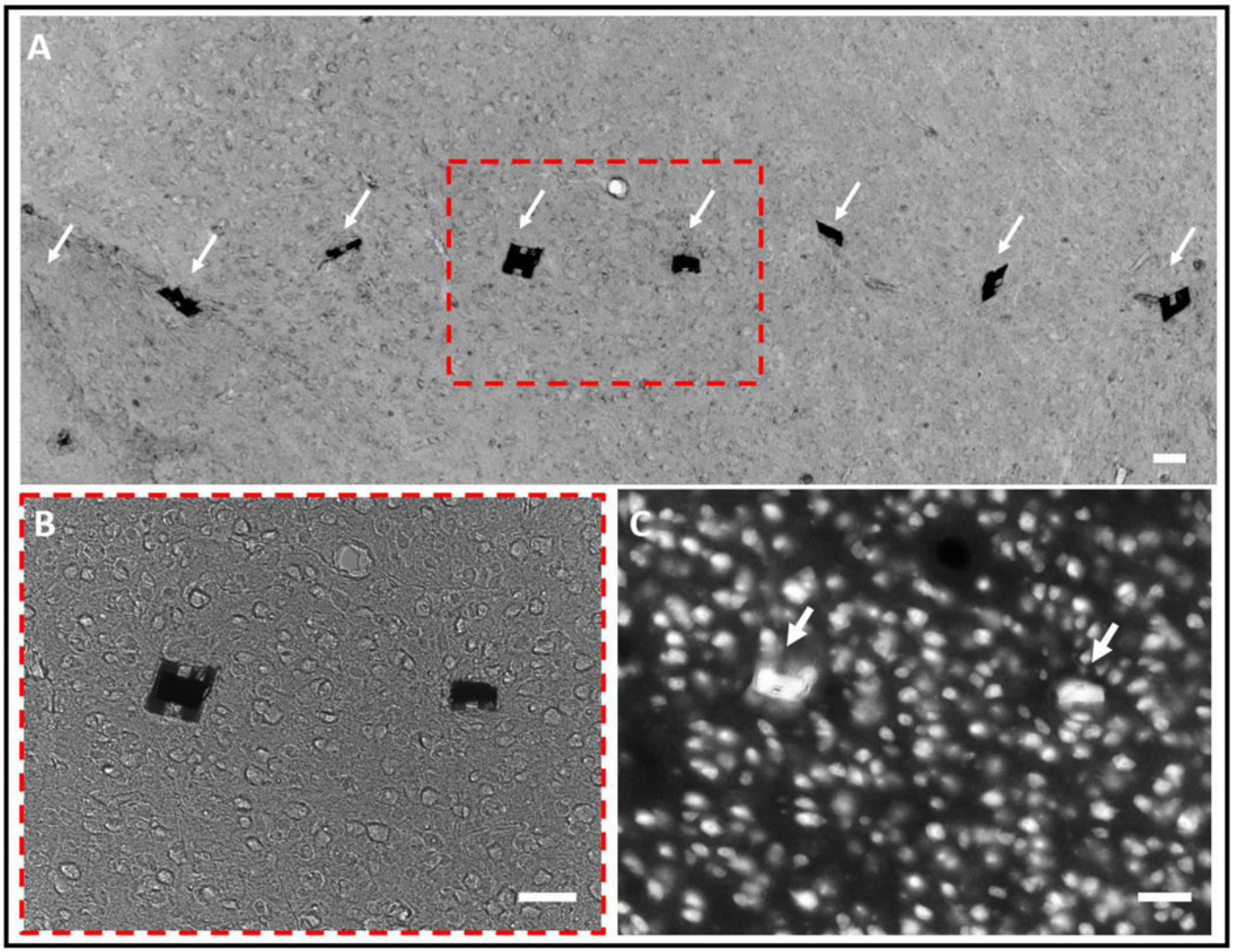

Figure 8:

Tissue-NET interface two months after implantation. (A) Bright-field image of a tissue slice (20 μm thick) in the mouse cortex where an 8-shank NET probe was implanted. The arrows highlight the implanted locations of the NETs, in which one out of eight was dragged out during tissue slicing. (B) Zoom-in view of the dashed box in (A), showing that the tissue morphology near the NETs was normal. (C) Fluorescent image of the same tissue slice where neuron cell bodies were fluorescently labeled. Scale bars: 50 μm.